AIP | Journal of Applied Physics

Micro-manipulation using rotational fluid flows induced by remote magnetic micro-manipulators

Zhou Ye, Eric Diller, and Metin Sitti

Citation: J. Appl. Phys. **112**, 064912 (2012); doi: 10.1063/1.4754521
View online: http://dx.doi.org/10.1063/1.4754521
View Table of Contents: http://jap.aip.org/resource/1/JAPIAU/v112/i6
Published by the American Institute of Physics.

Micro-manipulation using rotational fluid flows induced by remote magnetic micro-manipulators

Zhou Ye,[a] Eric Diller,[b] and Metin Sitti[c]
Department of Mechanical Engineering, Carnegie Mellon University, Pittsburgh, Pennsylvania 15213, USA

(Received 27 March 2012; accepted 24 August 2012; published online 27 September 2012)

We present a non-contact manipulation method for micron scale objects using locally induced rotational fluid flows created by groups of untethered magnetic micro-manipulators. The magnetic micro-manipulators are rotated in a viscous fluid by an externally generated magnetic field to create rotational flows, which act to move micro-objects in the flow region. One single spherical micro-manipulator is used to manipulate one object at a time, while an array of micro-manipulators spin in synchrony on a surface patterned with magnetic micro-docks to create reconfigurable fluidic channels for simultaneous transportation of multiple objects. The induced rotational flow field and the resulting hydrodynamic forces on the micro-objects are studied using both finite element solutions and analytical models from previous studies. These results are compared with experiment to determine manipulation characteristics for the complex flows. Due to its untethered and non-contact operation, this micro-manipulation method could be used to quickly move fragile or non-fragile micro-objects in inaccessible or enclosed spaces such as in lab-on-a-chip devices. © *2012 American Institute of Physics*. [http://dx.doi.org/10.1063/1.4754521]

I. INTRODUCTION

The ability to handle objects at the micron scale plays a crucial role in many applications including microfluidics, biological and colloidal science, lab-on-a-chip systems, and micro-assembly. Based on the mobility of a given micro-manipulator, currently available micro-manipulation techniques can be subdivided into two categories. The first approach uses mobile agents or end-effectors, and manipulates micro-objects by controlling the motion of such devices. Optical tweezers,[1–3] magnetic tweezers,[4,5] micro-grippers,[6,7] externally controlled bacteria,[8] and untethered micro-robots[9–20] fall into this category. Fine manipulation resolution can be achieved by these techniques, but they are limited by their workspace, manipulation speed, and ability to manipulate many micro-objects in parallel. The other category involves locally patterned surfaces or structures, including dielectrophoresis,[21,22] electrophoresis,[23] optical arrays,[24,25] and microfluidic devices, including use of micro-pumps/valves or magnetophoresis.[26–28] These techniques can achieve simultaneous manipulation of large numbers of micro-objects, but lack versatility due to their strict requirements for highly structured and specialized environments such as patterned surfaces or delicate three-dimensional structures, which are not possible to reconfigure *in situ*.

In this study, we propose a new non-contact micro-manipulation method using a single spherical magnetic mobile micro-manipulator to enable high precision and long-distance non-contact manipulation tasks with versatility in fluidic environments. In this case, the proposed method achieves the advantages of the first category of fine manipulation resolution and improves on manipulation speed. In addition, by introducing a specially prepared surface, multiple stationed magnetic micro-manipulators can work in parallel to transport multiple objects simultaneously. This achieves the advantages of the second category, but in this case the stationed positions of the manipulators are variable, maintaining the versatility of the first category. Magnetic micro-manipulators are rotated by an external magnetic field to generate rotational flow fields, which propel micro-objects via fluidic drag forces for precise non-contact manipulation and long-range transportation of individual micro-objects on a planar surface. Rotation of a single mobile spherical micro-manipulator results in both rotational fluid flow and two-dimensional mobility of the manipulator due to its rolling-sliding-based locomotion. Therefore, rotation of the manipulator can be used to achieve fast, long distance, and precise displacement of micro-objects with no contact from the manipulator. In this simple case, no specialized surface is required to perform manipulation tasks, and the micro-object being manipulated moves closely along with the mobile magnetic micro-manipulator. As a second more advanced case, multiple micro-manipulators are proposed to work in parallel on a surface patterned with magnetic micro-docks to create reconfigurable virtual fluid channels for concurrent, non-contact transportation of multiple micro-objects. The simplicity of the proposed mechanism, the mobility of the magnetic micro-manipulators, as well as the flexibility of the virtual fluidic channels generated by the micro-manipulator array impart versatility to this manipulation method for various manipulation tasks.

Manipulation methods using rotating manipulators have been reported before. A contact-based manipulation method using a nano-wire to transport a micro-object near a patterned solid surface was first demonstrated.[29] Using a similar nano-wire as the manipulator, a non-contact fluid-based

[a]zhouye@andrew.cmu.edu.
[b]ediller@cmu.edu.
[c]sitti@cmu.edu.

manipulation method was also demonstrated.[30] The concept of using multiple manipulators to create virtual fluidic channels was also introduced in our previous study.[31] However, fluid conditions required for successful manipulation were not considered in either work. In this study, we demonstrate successful manipulation of micro-objects based on the proposed mechanism using not only a single manipulator but also multiple manipulators for parallel manipulation, and give a detailed analysis of the mechanism and the object's motion in the induced rotational fluid field.

Manipulation of sub-millimeter scale objects is experimentally demonstrated, and the rotational flow field induced by a rotating spherical micro-manipulator is studied by numerical simulations. In addition, the motion of objects with different sizes and shapes in the induced rotational flow field is characterized by experiments and analyzed qualitatively. We particularly look into the stable orbiting motion of objects in the induced rotational flow, based on which our proposed manipulation mechanism is implemented. Following from the simulations and experiments, we conclude that the proposed method is suitable for non-contact object manipulation in the low Reynolds number (Re) regime, and investigate the object size range over which they can be accurately manipulated.

II. DESCRIPTION AND MODEL

The proposed non-contact micro-object manipulation method, based on locally induced rotational fluid flows, can be implemented with either one single or multiple magnetic micro-manipulators for various manipulation purposes.

A. Rotating magnetic micro-manipulators

We first consider the case of a single micro-manipulator spinning in contact with a flat substrate in a fluid environment. Control of the position of the micro-manipulator can be achieved by varying the magnetic field rotation axis. Normally, the micro-manipulator rotates about an axis perpendicular to the substrate. To induce translational manipulator motion, the rotation axis is tilted from vertical by a small angle, creating a rotation component $\Omega_{\parallel}$ parallel to the substrate. This parallel rotation component results in translational locomotion of the magnetic manipulator on the substrate, while the remaining perpendicular component $\Omega_{\perp}$ generates the rotational fluid flow for micro-object manipulation.[31] The perpendicular spinning rate $|\Omega_{\perp}|$ of the manipulator determines the rotational flow velocity of the surrounding field, and due to the low Re environment, has a linear influence on the circulating speed of the micro-object around the manipulator. In this way, coarse and fine manipulation of the object can be achieved by controlling the rotation speed, which can be controlled to any speed up to hundreds of Hz. After the object is placed at the target position, pure rolling is applied ($\Omega_{\perp} = 0$) for the manipulator to slowly roll away from the object without introducing disturbance to the positioned object.[16]

To achieve precise control of multiple micro-manipulators, a special substrate with magnetic micro-docks embedded in prescribed positions is used.[31] The micro-docks act as magnetic traps for the magnetic micro-manipulators. First, each magnetic manipulator, one after another, is moved towards a target micro-dock by a previously demonstrated method.[32] After multiple manipulators are trapped in fixed positions by the micro-docks, all manipulators are driven simultaneously by an applied rotational magnetic field to form the virtual fluidic channels. The trapped micro-manipulators can be independently addressed to new positions by a previously demonstrated multi-robot control method (see supplementary material),[33] and hence the virtual fluidic channels are reconfigurable during operation. In short, this method relies on micro-manipulators with slightly different magnetization values to achieve independent addressing using low-strength rolling magnetic fields. This relies on the unique magnetization values being separated at least by a factor of roughly 10%. In order to maintain a large level of magnetic torque for spinning actuation, the magnetization values are kept as high as possible while maintaining addressability. In low Re environments, the flow velocity far from the rotating manipulators generated by multiple manipulators can be approximated by the linear sum of the flow fields generated by each single magnetic manipulator. This means that results from the study of single manipulator can be simply extended to the case of multiple manipulators.

B. Modeling

1. Numerical modeling of the induced rotational fluid flow

Understanding the flow field generated by a rotating magnetic manipulator is crucial for precise or automated manipulation. Such understanding can be readily extended to multiple-manipulator cases given the linearity of fluid flows in the low Re regime. Stokes flow analytical solutions are available for the case of a sphere rotating in an unbounded liquid,[34] but the presence of the underlying substrate retards the fluid flow and thus significantly deviates the flow field from the Stokes flow case. Therefore, finite element simulations (details in supplementary material[45]) were carried out for the case of a 360 μm-diameter sphere spinning at $\Omega_{\perp} =$ 50 Hz on the bottom surface of a 30 mm $\times$ 30 mm $\times$ 1 mm container filled with liquid of kinematic viscosity 50 cSt (rotational Re is 0.20). High viscosity oil is chosen to reduce Re, and to keep the results valid for smaller scale manipulators. The results, presented in Fig. 1(a), show a steady-state flow velocity taken from the equatorial plane of the rotating sphere with a power law flow velocity fall-off on the plane fitted from the data as

$$|v_{flow}| = |\Omega_{\perp}| R \left(\frac{R}{r}\right)^{2.43}, \quad (1)$$

where R is the radius of the sphere and r is the distance to the position of interest from the sphere center. Results of multiple simulations with variations either in viscosity or sphere size validate this relationship and demonstrate that Eq. (1) is valid in the Re < 1 regime.

Due to inertial forces being comparable to viscous forces for Re beyond unity, non-tangential velocity

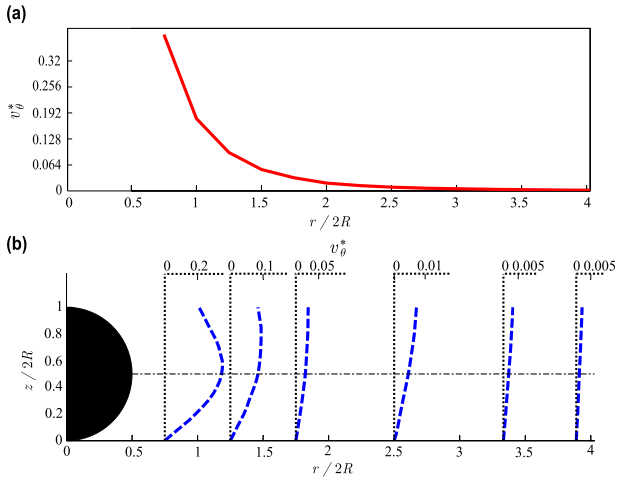

FIG. 1. Tangential velocity (v_θ) data from finite-element simulations taken from a half x–z plane ($z/2R \in [0, 1]$) which cuts through the cross-section of the spinning sphere (represented by the solid dark semicircle in the figure). All velocities are normalized by the linear speed of the spinning sphere at its equator ($\Omega_\perp R$) as v_θ^*. (a) The solid curve shows v_θ^* as a function r at $z/2R = 0.5$ (the equator plane of the manipulator). The curve indicates a power law fall-off of v_θ^* with respect to r, and a fit to the data from the curve is given by Eq. (1). (b) v_θ^* vs. height z, is given at some selected distances r, showing the profile evolving from highly nonlinear in the neighborhood of the sphere to linear far from the manipulator. The tangential velocity data used to plot the curves are scaled with different scaling factors, which is 20 at the smallest r, 40 at the larger two r's, and 200 at the largest three r's.

components, the radial (v_r), or vertical (v_z) velocity components, can be significant. The liquid in the neighborhoods of the poles of the sphere is drawn towards its equator following spiral paths,[35] with the developed flows being ejected away from the sphere close to its equator. However, this equatorial flow ejection, which results from inertial effects, becomes small compared to the circumferential flow velocity v_θ as Re becomes smaller than unity. Finite element analysis shows that for the range of Re considered here in this work (Re < 1), the relative magnitude of the radial component is $v_r/v_\theta < 0.01$, indicating that the radial flow, and hence the corresponding radial fluidic viscous drag, is negligible when analyzing the behavior of the objects during manipulation.

2. Motion of micro-objects in the induced rotational fluid flow

The behavior of non-neutrally buoyant micro-objects in the locally induced rotational flow field is the result of contributions from viscous drag, buoyant weight, shear-induced forces (radial and vertical), added mass force, and interaction between surfaces such as adhesion and surface friction.[36] The strong dependence of the hydrodynamic forces on the flow velocity distribution as well as the complex coupling between these forces in a highly non-linear three-dimensional flow field makes it difficult to analytically model the precise behavior of micro-objects in the induced rotational flow field. For non-contact manipulation purposes, we analyze one significant motion bifurcation: when an object circles in a stable manner within the neighborhood of the rotating manipulator rather than being ejected away. This is because that the proposed mechanism requires the objects being manipulated to be held in orbit. Based on our analysis in force balance, the conclusion is drawn that two criteria need to be met to enable stable orbiting behavior of the object in the rotational flows:

- *Motion criterion*: For an object resting on a substrate, mechanical contact with the underlying surface would occur when the surrounding fluid is at rest. When a rotational flow field is induced by a nearby rotating magnetic manipulator, a lifting effect is exerted onto the object due to a non-uniform distribution of flow velocity in the z direction (see Fig. 1(b)).[37] If the rotational flow field is strong enough, such a lifting effect could overcome the weight of the object and the adhesion between the object and the substrate, and thus lift the object from contact with the substrate.[38] If such lift-off occurs, then the object would tend to move with the surrounding flow without surface contact; if lift-off does not occur, then to initiate micro-object movement, the propelling viscous drag force experienced by the object must overcome the surface friction.
- *Orbiting criterion*: To hold the object in a circular orbit rather than being ejected radially from the micro-manipulator, the required centripetal force must be supplied by the total contribution from radial hydrodynamic forces and surface friction if the object is in contact with the substrate. As shown in Fig. 2, the radial shear-induced force points towards the rotation center where the tangential flow velocity is higher[39] and thus would be the major hydrodynamic force to provide the centripetal force. A more detailed analysis is given in the following section.

It should be noticed that the *motion criterion* is a necessary but not sufficient prerequisite to the *orbiting criterion*.

3. Forces on micro-objects

The major forces acting on a micro-object in the induced rotational flow field are shown in the free body diagram of Fig. 2. While the object shape studied in this section is a sphere, the results can apply roughly to other shapes as well through similar analysis. The following terms are predefined: ρ_{obj} and ρ_{fl} are the density of the object and the

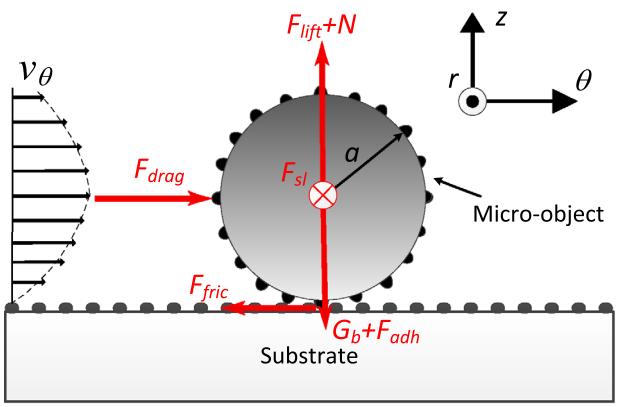

FIG. 2. Free body diagram of a spherical micro-object in contact with the substrate in the induced rotational flows when viewed along the radial axis, ignoring radial and vertical fluidic drag forces. The microscopic roughness on the object and the substrate is enlarged.

surrounding fluid, respectively. a is the radius of the micro-object, ν is the kinematic viscosity of the fluid, u_c is the flow velocity at the position of object's center, v_{obj} is the velocity of the object, γ_r is the shear rate along the radial direction of the flow field, and γ_z is the shear rate along the vertical direction. The centripetal force with added mass effect required to hold a spherical object in a circular orbit is given as[40]

$$F_{cp} = \frac{mv_{obj}^2}{r} = \frac{\left(\rho_{obj}\frac{4\pi}{3} + \rho_{fl}\frac{2\pi}{3}\right)a^3 v_{obj}^2}{r}. \quad (2)$$

Order of magnitude analysis with SI units gives $F_{cp} \sim 10^{-10}$ N for $r = 3R$ and $F_{cf} \sim 10^{-14}$ N for $r = 8R$. Precise modeling of the shear-induced force, even only in the radial direction, is difficult when the object is in contact with the surface as the flows are highly non-uniform functions of r and z (see Fig. 1). For a qualitative analysis, the velocity gradient in the z-direction is neglected, while Eq. (1) is used for the radial gradient, as the derivative with respect to r gives the shear rate γ_r. Because the flow velocity at the equator height gives the maximum shear force in the region, this result is interpreted as an upper bound.[39]

$$F_{sl} = \rho_{fl}\nu^{\frac{1}{2}}a^2(u_c - v_{obj})|\gamma_r|^{\frac{1}{2}}, \quad (3)$$

which gives $F_{sl} \sim 10^{-8.5}$ N for $r = 3R$ and $F_{sl} \sim 10^{-11}$ N for $r = 8R$. Therefore, at any distance r within the discussed range ($3R$–$8R$), the upper limit of F_{sl} is shown to be several orders of magnitude larger than F_{cp}, suggesting F_{sl} to be the main contributor to F_{cp}. In actual operations, F_{sl} should equal F_{cp} to hold an object in a stable orbit.

At a given distance from the manipulator r, the required centripetal force F_{cp} is proportional to a^3 and v_{obj}^2, while the shear-induced force $F_{sl} \propto a^2$. Because a smaller object has both smaller a and v_{obj} than a larger one, it is expected that smaller objects would more easily satisfy the orbiting criterion.

As previously stated, lift-off plays an important role in the satisfaction of the *motion criterion*. Therefore, let us first consider a typical case of vertical forces experienced by a spherical object resting on the substrate. These forces include the object's buoyant weight, adhesion between surfaces, and the hydrodynamic lifting effect. The buoyant weight is simply given by

$$G_b = (\rho_{obj} - \rho_{fl})g\frac{3}{4}\pi a^3, \quad (4)$$

and the hydrodynamic lifting effect can be approximated by[38]

$$F_{lift} = 9.26\gamma_z \mu a^2\left(\frac{\gamma_z a^2}{\nu}\right). \quad (5)$$

This approximation is formulated based on linear shear flow, which has a shear rate smaller than that of the actual induced rotational flow in the vertical direction, and thus should give a lower bound on the actual lifting effect. For an object at a given distance r, such a lifting effect would be the largest just before the object begins to move, because any translational or rotational motion of the object in a shear flow will significantly decrease the lift force.[38] Once the object starts moving, additional terms due to translation and rotation of the object should be added to Eq. (5) for proper approximation.[38]

Given the same weights, spherical objects resting on a flat plane would experience smaller adhesion from the plane than objects with other shapes due to the smaller contact areas. According to the Johnson-Kendall-Roberts (JKR) model of elastic contact between a smooth sphere and a smooth flat surface, the pull-off force required to lift a sphere from a flat surface is determined as[41]

$$P = 1.5\pi a W, \quad (6)$$

where W is the work of adhesion between the object and the substrate immersed in the given fluid. Lift-off occurs only if

$$F_{lift} - G_b > P. \quad (7)$$

Due to typical micron scale roughness of the surfaces, the actual pull-off force required could be more than one order of magnitude smaller than P.[42]

Once lift-off occurs and surface friction vanishes, an object will be driven at a non-zero translation speed by the rotational flow, determined by hydrodynamic effects. The flow field is highly non-uniform (see Fig. 1), which results in complex hydrodynamic interactions. However, Taylor's expansion technique can be used to approximate any general flow field with the presence of a wall by second-order polynomial flow fields, in which case the viscous drag forces and torques on a sphere near a wall have already been examined.[43,44]

In cases where lift-off does not occur, mechanical contact between the object and the substrate causes surface friction, which would be a constant resistive force F_f. Such force is directly related to the actual contact area A_c as $F_f = \tau A_c$, where τ is the effective shear modulus between the object and the substrate. The inclusion of this force would tend to prevent objects from moving, and hence result in a larger difference between the object speed and the effective speed of the surrounding flow. If the total effect of the hydrodynamic forces fails to overcome F_f, the motion criterion is not met and the object will remain stationary.

III. EXPERIMENT, RESULTS, AND DISCUSSION

A. Experimental setup

The magnetic micro-manipulators used in this study are fabricated from a mixture of neodymium-iron-boron (NdFeB) particles (MQP-15-7, Magnequench) and polyurethane base (TC-892, BJB Enterprises), via a typical soft-lithography-based micro-molding process.[31] The substrate with embedded magnetic micro-docks is a spin-on-glass-coated (21F, Filmtronics) SU-8 substrate (SU-8 2050, Micro-Chem) with molded NdFeB docks. An electromagnetic-coil system (see Fig. 3), consisting of three orthogonal pairs of

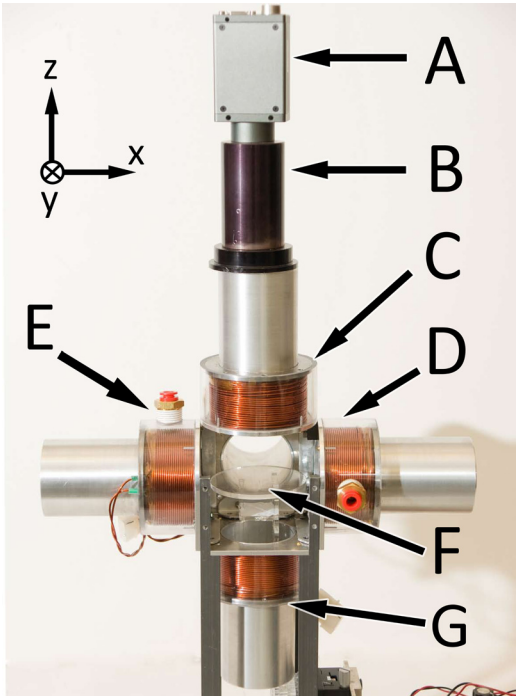

FIG. 3. Photograph of the electromagnetic-coil setup which contains six coils. A: camera for top-view vision feedback, B: microscope lens, C: top $+z$ coil, D: $+x$ coil (one of four horizontal coils), E: $-x$ coil, F: experiment workspace, G: bottom $-z$ coil. The $-y$ coil is removed to allow viewing of the workspace, and the $+y$ is behind the workspace seen from the view.

electromagnetic coils, is used to generate uniform magnetic fields to actuate and control the magnetic micro-manipulators.[31]

B. Results

All experiments are carried out in a 30 mm × 30 mm × 1 mm open-top container filled with silicone oil with a kinematic viscosity of 50 cSt to create a low Re environment. The magnetic field used to actuate the magnetic micro-manipulators has a field strength up to 5 mT supplied by the electromagnetic-coil system as shown in Fig. 3.

1. Demonstration of object manipulation

The capabilities of rotational micro-manipulator locomotion and non-contact micro-object manipulation are shown in Fig. 4(a), where a 360 μm-diameter magnetic spherical micro-manipulator transports a 200 μm-diameter polystyrene bead with a density of 1.05 g/cm on a glass substrate. An external magnetic field with strength of 3.5 mT rotating at a frequency of $|\Omega| = 30$ Hz was applied to induce the synchronous rotation of the magnetic manipulator. In this experiment, the rotation tilt angle was kept small ($<10^{\circ}$), resulting in a translational manipulator speed of approximately 2.5 manipulator-diameters per second. During manipulation, the micro-object was trapped in orbit along with the traveling manipulator as it translated, resulting in a stable "carrying" behavior for long-distance manipulation. A video of feedback-controlled automated coarse/fine positioning and release of a 200 μm-diameter polystyrene micro-bead is demonstrated in the supplementary material.

The concept of using multiple rotating micro-manipulators in parallel to create virtual fluidic channels for non-contact object transportation is illustrated in Figs. 4(b) and 4(c). Due to the complex flow field generated by multiple manipulators, a critical separation between the polystyrene bead and the closest manipulator was observed, within which the beads were trapped in orbit around the single manipulator instead of being passed to the next one. The value of such a critical initial separation depends on the spacing between manipulators. In this experiment, the distance between the spinning manipulators was 1200 μm, resulting in a critical initial separation of about 600 μm. Configurations of micro-manipulators other than a straight line or "L" shape are feasible.

2. Characterization of object speed

Experimental measurements, shown in Fig. 5, were taken for object speed v_{obj} as a function of radial distance r from the micro-manipulator center for several sizes of spherical and non-spherical objects. Polystyrene beads of two different diameters (200 μm and 116 μm), 400 μm polyurethane arrows and 600 μm polyurethane blocks were tested. The largest distance r that gives a non-zero v_{obj} for a certain object, designated as r_m, defines the range within which the *motion criterion* is satisfied for the corresponding object, whereas satisfaction of the *orbiting criterion* is not directly seen from the figure.

Experimental results suggest a strong influence of the object size and shape on both the satisfaction of the *motion criterion* and the object speed. The previous qualitative force analysis in the modeling section is helpful to explain these experiment results. First, it is observed that shapes closer to spheres give a larger r_m. This may directly result from the fact that the other shapes tend to lie flat on the substrate, increasing contact area and thus adhesion, leading to the failure for occurrence of lift-off and significant surface friction. Next, at a giving distance r, the larger spherical objects orbit with higher speeds than non-spherical objects for small values of r. This is because, for spherical objects experiencing much less adhesion than the arrows and the blocks, it is possible for them to be lifted off from the substrate when they are placed close to the rotating manipulator, which is also the center of the rotational flow field. According to the previous analysis, after lift-off occurs, surface friction is no longer present, resulting in higher steady object speeds than that with the presence of surface friction. Third, the smaller sphere moves significantly slower than the larger ones at any given r within the range of experiments. Noticing that F_{lift} is explicitly proportional to a^4, while $P \propto a$ and $G_b \propto a^3$, the lifting effect varies most significantly with object size, which means that a sphere with a larger size is easier to lift off from the surface. Once lift-off occurs, a larger F_{lift} will lead to a wider separation between the object and the substrate; as the separation increases, the influence of the substrate on hydrodynamic effects which retards object movement decreases logarithmically for very small gaps.[43,44] In addition, because v_θ is a function of z (see Fig. 1(b)), smaller objects are subject to a smaller v_θ and thus weaker overall

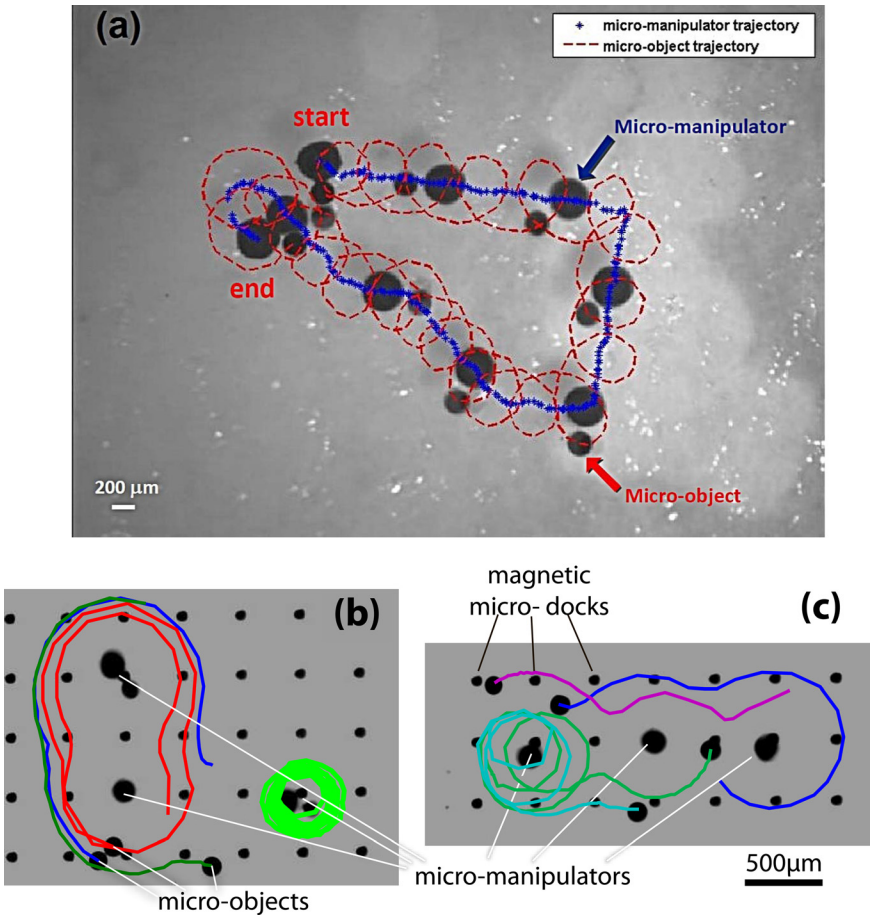

FIG. 4. (a) Top-view optical microscope images of a 365 μm-diameter spherical magnetic micro-manipulator carrying a 200 μm-diameter polymer micro-bead along an arbitrary path on a glass substrate using rotational fluid field. Eight frames taken from video of the whole manipulation process, with an equal interval of 1.23 s between each of them, are overlaid to show the paths of the micro-manipulator and polymer bead. The entire duration is 9.87 s. Three magnetic micro-manipulator rotates at 30 Hz and translates at a speed of approximately 2.5 manipulator-diameter per second, (900 μm s^{-1}). (b) and (c) The micro-manipulators are trapped at prescribed positions by magnetic micro-docks embedded in the substrate while rotating at 50 Hz in (b) "L"-configuration and (c) line-configuration. The same manipulators are used in both configurations, showing the versatility of the method. The images are frames taken from video of the manipulation of multiple micro-objects. The colored lines show the actual trajectories of multiple micro-objects being simultaneously manipulated from different starting positions.

hydrodynamic propulsion. This may also help to explain why the smaller spheres move with the lowest speed at very small values of r, within which distance the flow velocity varies drastically with z.

Although not directly shown in Fig. 5, it has been observed in the experiments that the object size plays a major role to determine the satisfaction of the *orbiting criterion*. For the larger beads, ejection was observed above a critical distance, while the smaller beads always remained in orbit, an effect predicted in Sec. II B 3 from looking at a scaling analysis. In the extreme case where the object's size is significantly smaller than the manipulator's, the object tends to be drawn to the manipulator rather than maintaining a stable distance (supplementary material video shows the 116 μm-diameter beads being drawn into contact with the manipulator). For precise manipulation of fragile or biological micro-objects, it could be disadvantageous if the objects are drawn too close to the manipulator and eventually in contact.

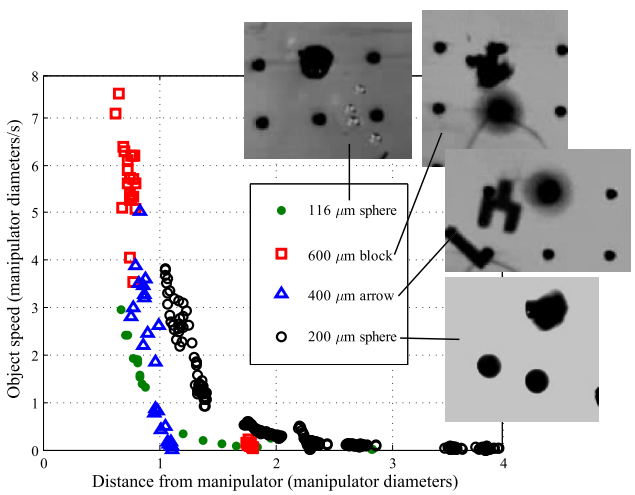

FIG. 5. Experimental micro-object speeds as a function of distance from a single 360 μm-diameter micro-manipulator spinning at 50 Hz. Data points were extracted at 10 Hz from 30 s of video for each object, and distance is normalized by the manipulator diameter. Data points stop at the distance when the object speed reaches zero. The insets are an image of each object type being manipulated, taken by optical microscope.

Synthesizing the effect of both object shape and size into a usable heuristic, we propose that this rotation-based micro-manipulation method will result in reliable manipulation or transportation of both spherical and non-spherical objects satisfying both manipulation criteria for object sizes in the range

$$0.5 < \frac{r_{obj}}{r_{manip}} < 1, \tag{8}$$

where r_{obj} is the characteristic size of the micro-object to be manipulated, and r_{manip} is the characteristic size of the magnetic micro-manipulator. For spherical objects and manipulators, r_{obj} and r_{manip} are a and R, respectively. As long as the relationship of sizes of both the manipulators and the objects satisfies Eq. (8), the proposed mechanism would be expected to work for systems down to a few microns and in various

liquids, such as water.[30] However, as the size decreases to the nano-scale, Brownian motions would be more significant and the applicability of the proposed method on such small scale requires further investigation.

IV. CONCLUSION

In conclusion, we demonstrated a robust method for non-contact manipulation and long-range transportation of sub-millimeter-scale objects on a planar surface using rotational flows generated by rotating spherical magnetic micro-manipulators. Based on simulation and experimental results, such a method can be applied to various manipulation tasks on smaller scales down to micro-scale or in different liquids as long as the following conditions are satisfied: (1) Reynolds number is low ($Re < 1$) and (2) the ratio of object size to manipulator size is between 0.5 and 1. Two different operating modes of the proposed mechanism were introduced for various object-handling demonstrations. In the first mode, a single mobile micro-manipulator was used for both fast, long-range transportation and fine positioning of one micro-object at a time without a specialized patterned surface. In the second mode, multiple micro-manipulators were trapped at prescribed positions by the underlying magnetic micro-docks embedded in the substrate and spun simultaneously to create virtual fluidic channels for object-manipulation. These virtual fluidic channels could be reconfigured simply by changing the arrangement of the micro-manipulators. The proposed method has advantages over existing micro-manipulation schemes in liquids by allowing parallel, untethered, and non-contact manipulation with course and fine precision capabilities in constrained spaces with no damage to the micro-objects being manipulated. In addition, comparing to those well-accepted parallel manipulation schemes such as dielectrophoresis and electrophoresis, the proposed method has the capability to reconfigure manipulation paths *in situ* without changing the patterned substrate. However, contact-based micro-manipulation methods such as microgrippers could be better when larger manipulation forces or dexterous assembly of parts are required. The proposed method is also not as capable as methods like dielectrophoresis and electrophoresis to simultaneously handle very large numbers of micro-objects. Future work will involve the use of the proposed methods for non-contact manipulation in microfluidic channels.

ACKNOWLEDGMENTS

The authors thank Shuhei Miyashita and all the members of the NanoRobotics Laboratory for all their support and suggestions.

[1]D. Grier, Nature **424**, 810 (2003).
[2]A. Ashikin, J. Dziedzic, and T. Yamane, Nature **330**, 769 (1987).
[3]Y. Jiang, Y. Matsumoto, and Y. Hosokawa, Appl. Phys. Lett. **90**, 061107 (2007).
[4]J. Yan, D. Skoko, and J. Marko, Phys. Rev. E **70**, 011905 (2004).
[5]H. Lee, A. Purdon, and R. Westervelt, Appl. Phys. Lett. **85**, 1063 (2004).
[6]M. Carrozza, P. Dario, A. Menciassi, and A. Fenu, in IEEE International Conference on Robotics and Automation, Leuven, Belgium (1998), p. 1811.
[7]D. Kim, B. Kim, and H. Kang, Microsyst. Technol. **10**, 275 (2004).
[8]S. Martel, C. Tremblay, S. Ngakeng, and G. Langlois, Appl. Phys. Lett. **89**, 233904 (2006).
[9]B. Donald, C. Levey, and I. Paprotny, J. Microelectromech. Syst. **17**, 789 (2008).
[10]H. Maruyama, T. Fukuda, and F. Arai, in *IEEE International Conference on Intelligent Robots and Systems*, St. Louis, MO, USA (2009), p. 1413.
[11]B. Behkam and M. Sitti, Appl. Phys. Lett. **90**, 023902 (2007).
[12]B. Behkam and M. Sitti, Appl. Phys. Lett. **93**, 223901 (2008).
[13]V. Arabagi, B. Behkam, E. Cheung, and M. Sitti, J. Appl. Phys. **109**, 114702 (2011).
[14]C. Liu, C. Chiang, C. Chang, and C. Liu, Sens. Actuators, A **130**, 545 (2006).
[15]C. Pawashe, S. Floyd, and M. Sitti, Appl. Phys. Lett. **94**, 164108 (2009).
[16]C. Pawashe, S. Floyd, E. Diller, and M. Sitti, IEEE Trans. Rob. **28**, 467 (2012).
[17]S. Floyd, C. Pawashe, and M. Sitti, IEEE Trans. Rob. **25**, 1332 (2009).
[18]M. Sitti, Nature **458**, 1121 (2009).
[19]M. Sitti, IEEE Rob. Autom. Mag. **14**(1), 53 (2007).
[20]D. R. Frutiger, K. Vollmers, B. E. Kratochvil, and B. J. Nelson, Int. J. Rob. Res. **29**(5), 613 (2010).
[21]P. Chiou, A. Ohta, and M. Wu, Nature **436**, 370 (2005).
[22]B. Taff, S. Desai, and J. Voldman, Appl. Phys. Lett. **94**, 084102 (2009).
[23]L. Kremser, D. Blaas, and E. Kenndler, Electrophoresis **25**, 2282 (2004).
[24]J. Curtis, B. Koss, and D. Grier, Opt. Commun. **207**, 169 (2002).
[25]D. McGloin, G. Spalding, H. Melville, W. Sibbett, and K. Dholakia, Opt. Commun. **225**, 215 (2003).
[26]L. Yeo, H. Chang, P. Chan, and J. Freind, Small **7**(1), 12 (2011).
[27]N. Pamme, Lab Chip **6**(1), 24 (2006).
[28]N. Pamme and C. Wilhelm, Lab Chip **6**(8), 974 (2006).
[29]L. Zhang, T. Petit, Y. Lu, B. E. Kratochvil, K. E. Peyer, R. Pei, J. Lou, and B. J. Nelson, ACS Nano **4**(10), 6228 (2011).
[30]T. Petit, L. Zhang, K. E. Peyer, B. E. Kratochvil, and B. J Nelson, Nano Lett. **12**, 156 (2012).
[31]E. Diller, Z. Ye, and M. Sitti, in *International Conference on Intelligent Robots and Systems*, San Francisco, USA (2011), p. 1291.
[32]C. Pawashe, S. Floyd, and M. Sitti, Int. J. Robot. Res. **28**, 1077 (2009).
[33]E. Diller, S. Floyd, C. Pawashe, and M. Sitti, IEEE Trans. Rob. **28**(1), 172 (2012).
[34]J. Happel and H. Brenner, *Low Reynolds Number Hydrodynamics: With Special Applications to Particulate Media* (Springer, 1973).
[35]Q. Liu and A. Prosperetti, J. Fluid Mech. **657**, 1 (2010).
[36]E. Nierop, S. Luther, J. Bluemink, A. Prosperetti, and D. Lohse, J. Fluid Mech. **571**, 439 (2007).
[37]P. Cherukat and J. Mclaughlin, J. Fluid Mech. **263**, 1 (1994).
[38]G. Krishnan and D. Leighton, Jr., Phys. Fluids **7**(11), 2538 (1995).
[39]P. Saffman, J. Fluid Mech. **22**, 385 (1965).
[40]L. Landau and E. Lifshitz, *Fluid Mechanics* (Pergamon, 1987).
[41]J. Israelachvili, *Intermolecular and Surface Forces* (Academic, 1992).
[42]K. Fuller and D. Tabor, Proc. R. Soc. London, Ser. A **345**, 327 (1975).
[43]L. Pasol, A. Sellier, and F. Feuillebois, Q. J. Mech. Appl. Math. **59**(4), 587 (2006).
[44]M. Chaoui and F. Feuillebois, Q. J. Mech. Appl. Math. **56**(3), 381 (2003).
[45]See supplementary material at http://dx.doi.org/10.1063/1.4754521 for experimental video showing the automated manipulation of single object using one manipulator, and transportation of multiple objects using an array of manipulators, corresponding to Fig. 4 and Fig. 5. Demonstration of rearranging in-situ the positions of two manipulators is also available.